Boron and Boron Carbide Materials: Nanostructures and Crystalline Solids

Kah Chun Lau, Yoke Khin Yap, and Ravindra Pandey

Abstract Owing to the rapid developments related to the novel $B_xC_yN_z$ ternary structures, the pedagogical review chapter has several antecedents as new results have emerged. Specifically, we will focus on the B_xC_y (with x, y = 0–1) hybrid material where the qualitative trend, in general, can be described by the ratio of its constituents. There is, however, a significant asymmetric popularity between the boron and carbon in the scientific literature. Carbon-based structures are well studied compared with boron-based structures. Consequently, understanding of the role played by boron in the formation of the B_xC_y hybrid structures remains somewhat incomplete. We, therefore, devote a substantial part of discussion on the boron-related structures with an aim to achieve the goal of a complete understanding of the physics and chemistry of the hybrid B_xC_y material.

1 Introduction

Advances in novel experimental techniques for fabrication and measurements together with development of new theoretical methods [1] have resulted, not only knowing the atomistic details of a given structural configuration, but fabrication of artificial structures that required placement of atoms at specified locations for tailor-made properties not exhibited by naturally occurring materials. The arrangements of atoms at nanoscale can now be routinely achieved. Both theoretical and experimental methods have observed a dramatic variation in the physical and chemical properties of a given material with the size at such length scale. For example, carbon exhibits novel properties in the form of clusters, fullerenes, graphene sheet, and carbon nanotubes (CNTs). Likewise, a large diversity in the topological configurations and properties of boron nanostructures has been reported.

K.C. Lau, Y.K. Yap, and R. Pandey (✉)
Department of Physics, Michigan Technological University, Houghton, MI 49931, USA
e-mail: pandey@mtu.edu

Y.K. Yap (ed.), *B-C-N Nanotubes and Related Nanostructures*,
DOI: 10.1007/978-1-4419-0086-9_9,

A brief yet fully readable account of the evolution of the so-called nanomaterials is beyond the scope of this review due to extraordinary diversity and many interconnections. Here, we restrict ourselves to highlight recent developments in the area pertaining to a hybrid system consisting of both boron and carbon atoms, B_xC_y. The B_xC_y hybrid structures can be considered as a subset of novel ternary hybrid structures, $B_xC_yN_z$ [2]. It is a well-known fact that synthesis of both B_xC_y and $B_xC_yN_z$ structures remains a challenge despite the publication of the first report in 1970s [3].

It is expected that the underlying structural and bonding configurations of the hybrid B_xC_y material will be related to the boron and carbon structures, thereby exhibiting properties generally derived from the constituent elements. It is therefore important to review the structural and bonding configurations of the boron and carbon solids and nanostructures. This is what we propose to do in the following sections summarizing the basic features and structural properties related to structures ranging from clusters to nanotubes to macroscopic crystalline solids. It will be followed by description of the hybrid boron carbide (i.e., B_xC_y). We will give a summary in Sect. 4.

2 Boron Allotropes: Solids and Nanostructures

2.1 Boron Solids

The understanding of the crystalline phases of the elemental boron solid is not yet fully established. Unlike carbon, bulk boron cannot be found in nature, and all the known boron allotropes were obtained experimentally. Within this context, boron solids can always be considered as fascinating candidates due to their varied polymorphism in the structural arrangements and complex interplay of the chemical bonding due to "electron deficiency" [4, 5]. Electron deficiency is defined as the case where the number of electrons is less than the available atomic orbitals in the valence configuration of an atom. The consequences [4–6] of an electron-deficient bonding in a given material may be summarized as follows: (1) The ligancy (i.e., coordination number) is higher than both the number of valence atoms and the number of valence orbitals. (2) In the lattice, adjacent atoms increase their ligancy to the values larger than the orbital numbers [6, 7]. Therefore, the term "electron deficient" simply suggests that novel structures based on elemental boron are expected to exist in nature. With insufficient electrons to support a structural configuration by conventional "two-electron two-center" bonds, the boron-based compounds generally tend to adopt a novel mechanism to resolve their *electron deficiency* through "two-electron multicenter" bonds, which are topologically connected in a complex networks [4, 5].

Relative to carbon, the crystalline phases of boron are among the most complex structures reported for a pure element [4, 8], which utilize the icosahedral B_{12} unit as a common structural component in the lattice. As shown in Fig. 1, the B_{12}

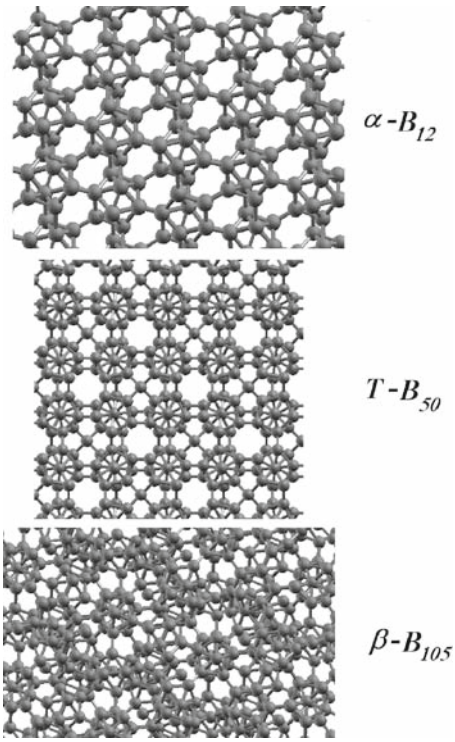

Fig. 1 Icosahedral unit-based crystalline boron solids: (*top*) α-B_{12}, (*center*) T-B_{50}, and (*bottom*) β-B_{105}

icosahedron can be interlinked by strong covalent bonds in a variety of ways to form several well-known polymorphs such as α-rhombohedral B_{12} (α-B_{12}) [9–17], α-tetragonal B_{50} (T-B_{50}) [11], or β-rhombohedral B_{105} (β-B_{105}) [9, 14, 16–19]. In spite of the existence of several crystalline phases, the relative stability between the various polymorphs and the phase diagram of solid boron needs to be studied [20].

It is interesting to note here that the B_{12} unit is a preferred building block satisfying the bonding requirement of boron atoms in a given lattice, though an isolated B_{12} cluster itself is not stable [21, 22]. To fulfill the electron deficiency in an isolated B_{12} unit [23, 24], boron atoms form triangles or polyhedra to share the electrons among themselves. For example in the α-B_{12} phase, a combination of localized covalent (i.e., two-center bonds) and delocalized multicenter bonds (e.g., three-center bonds) appear in the lattice. It can be interpreted as the preservation of the intrinsic stability of each individual icosahedron through the intra- and intericosahedral bonds in the crystalline lattice (Fig. 2). The energetically stable crystalline phases, α-B_{12} and β-B_{105}, are found to be semiconductors while the other metastable solid, T-B_{50}, interconnected by interstitial boron atoms (Fig. 1) is found to be a metallic conductor. Although comments have been made about nonmetal to metal

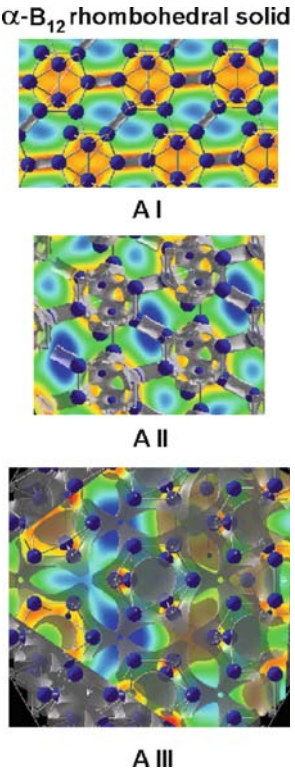

Fig. 2 The contour maps of the electron density of α-B_{12} (from *top* to *bottom*: AI, AII, and AIII) showing two-center (2c) and three-center (3c) bonds. The *red* region represents the high electron density contour, while the low electron density contour is shown by the *blue* region. The bonding is represented by the gray isosurface (AI-2c intericosahedral bond at 0.95 e/Å^3, AII-3c intraicosahedral bond at 0.77 e/Å^3, and AIII-3c intericosahedral bond at 0.60 e/Å^3) (reprinted with permission from [25], copyright American Chemical Society)

[14, 15] and nonmetal to superconductor [26–28] transitions, a detailed mechanism of the phase transition is yet to be reported.

2.2 Boron Nanostructures

In recent years, a large number of studies on various topological configurations of boron nanostructures, especially boranes [29–33], boron clusters [34–42], nanowires, nanoribbons, nanowhiskers, and nanotubes [43–45] continue to emerge. To understand the properties of boron nanostructures, discussions considering the basic features of distinctly reduced dimensionality and corresponding size-dependent studies are necessary and will be reviewed in the following section.

2.2.1 Boron Clusters

Analogous to the 0D carbon fullerenes, a search for the boron fullerene-like cage structures has yielded interesting results. Despite the B_{12} unit being the building

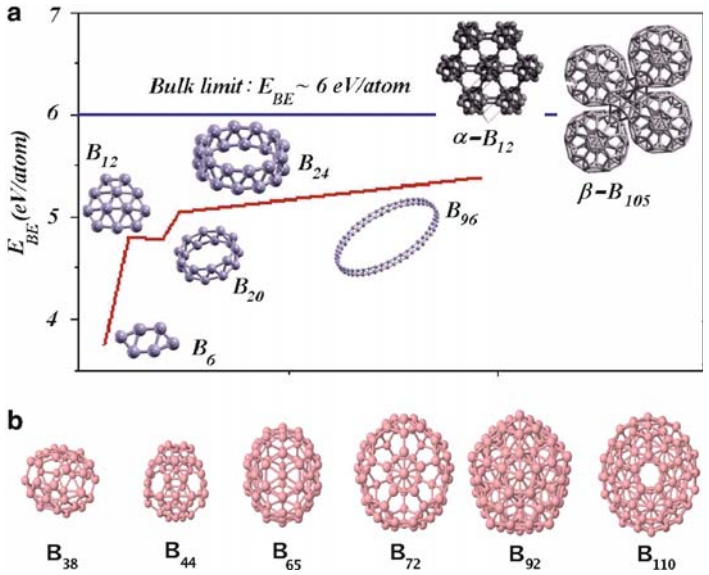

Fig. 3 (**a**)The 2D to 3D structural transition in boron clusters [48] (reprinted with permission from [48], copyright Brill Publishing Group), (**b**) The boron fullerene-like cage structure [49] (reprinted with permission from [49], copyright American Physical Society)

block for the boron solid, the clusters are generally found to prefer the structural motifs different from the B_{12} unit, such as 2D planar, quasi-1D tubular, or 3D double-ring [7, 42, 46–48] motifs shown in Fig. 3. One of the earliest experimental observation of the cluster [34] was a catalyst for a number of theoretical [38, 39, 46, 50–57] as well as further experimental [35–37, 40] studies on small boron clusters. Based on a series of photoelectron spectra in the small boron clusters regime, $B_n (n \leq 5)$ [41, 58–62], it is now generally accepted that boron and carbon form a set of complimentary chemical systems the bulk carbon is stable in 2D graphitic structure and the carbon clusters are characterized by 3D cages, whereas the bulk boron is characterized by 3D cages and the boron clusters are characterized by the 2D structures. The high stability of the 2D planar structures over the 3D structures is attributed to the presence of the effective electron delocalization on the bonds in the boron lattice [41, 48, 63, 64].

Although the boron clusters in the small clusters regime are well characterized, fewer studies are available for the large boron clusters [48]. To the best of our knowledge, the studies of large boron clusters mostly considered simple geometrical configurations with high symmetries, which do not resemble the fragments of either crystalline or amorphous bulk boron. Overall, the clusters favor the 2D planar structure up to 18 atoms and thereafter prefer the 3D tubular or double-ring structural motifs [42, 48, 65–69]. The 2D–3D structural transition observed at B_{20}, reminiscent of the ring-to-fullerene transition at C_{20} [70–72], suggests that B_{20} may be considered as the embryo of the thinnest single-wall boron nanotube [42].

Besides the 3D tubular or double-ring configuration, the boron cage structure, analogous to carbon fullerenes, has recently been proposed (Fig. 3), opening up the possibility of a completely new family of boron clusters with high stability in the large clusters regime. In spite of the instability of pristine B_{12} icosahedral cage, the boron fullerenes-like cages would be the second example in nature after the C_{60}-derived family, with a circular and distinct hollow structure. As has been pointed out earlier [49, 73], the most stable boron cages reach ~91% of the α-rhombohedral bulk stability. We note that the limit is ~89.9% for the large 3D double-ring isomer (i.e., infinite strip) whose stability tends to increase with the increase of the radius of the ring [48, 49, 68, 69, 73]. Among the boron fullerene-like cage B_n clusters with n = 12–300, the B_{80} fullerene-like cage, therefore, emerges as the most stable cluster with a gap of ~1 eV between the highest occupied and lowest unoccupied orbitals exhibiting an unusual high chemical stability.

The energetic competition among the 2D infinite strip together with the 3D double-ring and fullerene-like cage structures is expected to be reflected in the distinct features of chemical bonding present in the respective configurations. It is essentially an interplay between saturation of dangling bonds and the curvature strain associated with these 2D and 3D configurations. One now needs to address the question of their intrinsic structural stability via both experimental and theoretical studies of the vibrational and thermodynamic stability. Analysis of chemical bonding that governs the *electron-deficient* boron atoms in the large clusters also remains to be considered in future.

2.2.2 Boron Sheets

It is well known that CNTs are a structural paradigm for all tubular materials. CNTs can be seen as a cylindrical modification of graphite, which may geometrically be constructed by cutting a rectangular piece out of a single graphene sheet and rolling it up to form a nanotube. However, not a single direct clue can be found for boron nanotubes due to nonexistence of a boron sheet or graphitic-like boron layers in nature. Above all, studies on boron sheet configurations are limited only to theoretical ones that have been focused on the pristine 2D infinite plane and the corresponding finite-size planar structures. The understanding of the physics and chemistry of the layered crystalline condensed phase of boron remains to be an open question.

Assuming that the formation of BNTs can be analogous to CNTs that are formed only under kinetically constrained conditions, one can conjecture that: "*one of the main difficulties in synthesizing boron nanotubes appears to be the instability of a graphene-like boron sheet.*" Thus, while waiting for the empirical evidence, *first-principles* calculations [25, 74–79] have considered the question of the stability of the 2D boron sheets (Fig. 4). Taking the guidance from the finite 2D quasiplanar, convex, and planar boron cluster configurations [7, 48], several types of sheet configurations based on different structural motifs have been proposed. Instead of having the unsaturated dangling bonds as appearing in the finite 2D planar boron clusters, stability of the infinite 2D boron sheet can be attributed to the long-range

Coulomb forces embedded within its unique 2D crystalline lattice. Owing to the curvature strain, a boron sheet appears to be more stable than its curvature-derived nanostructures, namely fullerenes and nanotubes [73–75, 77, 79, 80].

Since the elemental boron solids have neither a purely covalent nor a purely metallic character, one can argue that the three-centered bonds and the electron-deficient features of boron [4, 5] should be energetically more competitive and stable than bonding features with only the sp^2 hybridization as found in the carbon graphitic system. Hence, the competing roles played by the three-centered and two-centered bonding in determining the stability of the 2D boron sheets were investigated [25, 74–79]. Among the possible configurations that have been studied [25, 76, 78], the α-boron sheet is found to be the most stable 2D planar boron sheet representing a combination of both three-centered and two-centered bondings [78, 79]. It is composed of both hexagonal and triangular motifs (Fig. 4) and the cohesive energy is about ~93% of the α-rhombohedral boron solid [78]. Interestingly, the results suggest that the pristine boron sheets should be metallic, irrespective of their different structural motifs [25, 74–79].

Following the α-boron sheet, the next stable configuration is the buckled triangular sheet [25, 74–77]. It was obtained from the geometry relaxation of a flat

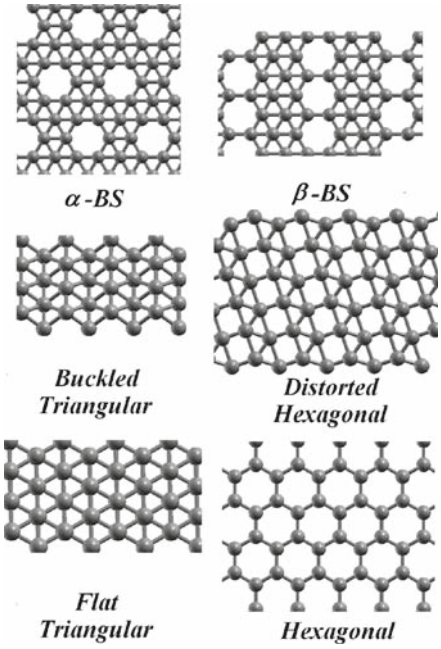

Fig. 4 The 2D pristine boron sheet configurations [25, 74–78]: (*top*) α-sheet and β-sheet (which are hybrid of hexagonal and triangular structural motifs), (*center*) buckled triangular and distorted hexagonal sheets (i.e., *triangle–square–triangle* {1221} sheet), (*bottom*) flat triangular and hexagonal sheets (reprinted with permission from [76], copyright American Chemical Society)

triangular sheet through a buckling along the perpendicular direction of the sheet. Subsequently, the buckling mixes in-plane and out-of-plane electronic states and can be thought of as a symmetry reducing distortion that enhances binding. Intuitively, the buckling of boron atoms is a response of the sheet to the internal stress imposed by the arrangement of the atoms in a perfect triangular 2D lattice. In an extensive first-principles study by Lau et al. [25, 76, 80], the results find a stable sheet configuration comprising a network of "triangle–square–triangle" units (i.e., {1221}) in the lattice. It was derived from a distorted hexagonal lattice of boron atoms. Similar to the α- and buckled triangular sheet configurations, the bonding in the distorted hexagonal sheet is characterized by both two-center and three-center bonds, reminiscent of the electron-deficient features of boron atoms [25, 76, 80]. Above all, the three-centered (i.e., perfect hexagonal sheet) or the two-centered bonded (i.e., flat triangular sheet) configurations [25, 74–77] are found to be energetically less favorable. Unlike carbon, the sp^2 bonding features are not preferred in boron sheets due to the partial occupancy of the in-plane sp^2 bonding states.

2.2.3 Boron Nanotubes

The predicted stability of the boron sheet configurations suggests, in principle, the feasibility of synthesis of boron nanotubes. In the scientific literature, there is only a single report [45] of synthesis of BNT showing that the synthesized 1D single-walled boron nanotubes (SWNT) are extremely sensitive to the high-energy electron exposure [45]. Thus, besides offering a new class of 1D nanostructures, the experimental study opened up many unanswered questions on the stability, energetics, and the electronic properties of the tubular boron structures [45]. Inspired by the so-called Aufbau principle proposed by Boustani [46], and partly stimulated by the experimental report, several theoretical studies have carried out the search for the stable tubular configurations of boron. Overall, the results find the stable nanotubes to be composed of different structures due to the several precursive competing boron sheet configurations from which the tubular configurations can be derived. Since the 2D boron sheets are metallic, the simple zone folding scheme suggests that SWBNTs should also be metallic, irrespective of their chiralities. Compared with the other 1D boron nanostructures, e.g., nanowires, nanoribbons, and nanowhiskers [43, 44], BNTs can be categorized as a new class of topological structure in boron [7, 77, 81]. While the boron nanowires, nanoribbons, and nanobelts are all found to be bulk-like (i.e., either in crystalline or amorphous phase) [43, 44, 82], details of the structural morphology of BNTs remain to be verified by experiments, in spite of the theoretical predictions of their stability [74, 75, 77, 79–81, 83–85].

It is interesting to note here that the finite size of boron tubular structures has also been predicted to be stable among other structural motifs [47, 66, 67, 73]. Spanning from B_{24} to B_{240}, the quasi-1D boron structures (Fig. 5) have been found to have a finite energy gap between the highest occupied and lowest unoccupied molecular orbitals [47, 66, 67, 73, 85]. As the cluster size and length of the tubular configurations increases, the configurational stability increases, but the energy gap

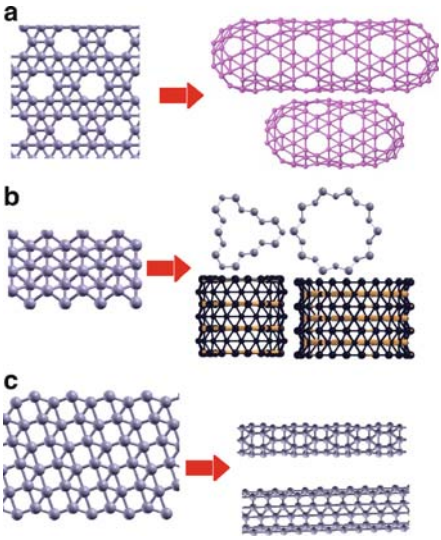

Fig. 5 The three most stable structural motifs of pristine 2D sheet: α-sheet, buckled triangular sheet, and distorted hexagonal sheet, and their corresponding pristine single-walled nanotubes with different chiralities [73–75, 77, 79–81]

decreases approaching to be metallic in the limit of infinite length [73, 85]. We note that the electron transport in BNTs is predicted to be ballistic [86].

Analogous to CNTs, details of the construction and classification of pristine infinite SWBNTs derived from the buckled triangular and distorted hexagonal sheets can be found following the scheme suggested by Kunstmann et al. [77, 81]. On the other hand, the construction and classification of the pristine SWBNTs derived from the α-sheet can be found in the recently published work [79]. The reported tubular configurations derived from energetically preferred α-, buckled triangular, and distorted hexagonal sheets (Fig. 5) show the stability that is about ~90–93% of the α-rhombohedral boron solid.

In contrast to the metallic boron nanotubes that derived from the buckled triangular and distorted hexagonal configurations [74, 75, 77, 80, 81, 84], the tubular configuration derived from the α-sheet shows variation in electronic properties with variation in the structural parameters [79]. For example, the energy gap of a small-diameter semiconducting nanotube decreases as we increase both the diameter and chiral angle of the tube. The nanotubes with diameter larger than 17 Å are predicted to be metallic as is the case with the α-sheet. Since small-diameter α-nanotube does not follow the simple zone folding scheme, one needs to examine the variation in the chemical bonding of the α-nanotube in going from small to large diameter. The diameter-dependent variation in the bonding features is likely to influence the electronic properties of α-nanotubes.

The crystalline bundles of BNTs have recently been the subject of a theoretical study [81] that found the bundles to be metallic. Considering the semiconducting nature of the boron crystalline solids [14], the metallic BNT crystalline bundles

appear to represent a new condensed phase of boron. For the case of the CNT bundles, the Van der Waals interaction between the pristine CNTs is comparable to that in the graphite layers [87, 88]. On the other hand, the BNTs are covalently bonded in the bundles via two-centered and three-centered bonds [81], reminiscent of the two-centered and three-centered bonds representing the intericosahedral interactions (Fig. 2) in the α-rhombohedral boron solid [13]. Likewise, one might expect the presence of the covalent bonds in multiwalled BNTs in contrast to the case of multiwalled CNTs where a weak coupling exists among the walls of nanotube formed by carbon. Under ambient condition, one can therefore say that the CNT bundles are sparse in the condensed crystalline phase, while the BNT bundles are expected to be in a close-packed crystalline phase. Hence, substantial differences related to the bulk properties of BNT and CNT bundles will be expected. For example, *first-principles* calculations on the BNT bundles [81] yield the modulus of compressibility (i.e., bulk modulus, B_0) to be ~85–111 GPa [81], higher than ~28–39 GPa of CNT bundles [87] but lower than ~185–220 GPa for boron solids [17, 89]. The Debye temperature of BNT bundles is predicted to be ~700–950 K at room temperature [81], compared with that of ~1,219 K for the β-boron solid [18].

3 Boron Carbide Allotropes: Solids and Nanostructures

Carbon and its related allotropes in both solids and nanostructures are generally well studied relative to boron and its compounds. In the synthesis of boron carbide allotropes, the role played by carbon is relatively overwhelming. Therefore, being a fundamental precursor for both solid and nano structures, the importance of carbon in the formation of B_xC_y allotropes seems to be unquestionable.

3.1 Carbon Solids

The most convenient classification scheme for the carbon polymorphs is based on the type of hybridization of the valence orbitals of carbon [90]. Since the energy differences between the valence orbitals (i.e., 2*s*, $2p_x$, $2p_y$, and $2p_z$) are small, the mixing of 2*s* with 2*p* bonding determines the structural and bonding properties of carbon solids. Consequently, the diversity of carbon allotropes is associated with the fact that carbon atoms may prefer sp^n (n = 1–3) hybridization [91, 92], rendering sp^3 (tetravalent), sp^2 (trivalent), and *sp* (divalent) bonds in a given lattice. Each valence state then corresponds to a certain form of an allotrope, such as (three-dimensional) spatial structure, diamond (sp^3), two-dimensional planar structure, graphite (sp^2), and the third possible state, one-dimensional chain-like carbyne (*sp*). For diamond, each carbon atom is sp^3 hybridized in the tetrahedral structure, arranged either in the cubic or hexagonal (wurtzite) polymorphs [93, 94].

In graphite, the sp^2 hybridization forms in-plane σ bonds whereas C-$2p_z$ orbitals prefer the arrangement of the hexagonal crystalline lattice resulting in weak bonding of the graphitic layers via the Van der Waals forces at the interlayer distance of ~3.5 Å [95]. Because of the subtle interlayer interaction, the energetic stability of these layered structures essentially depends on the stacking sequences of the individual graphene sheet. Among the four possible types of stacking sequences, namely the *ABAB* (i.e., the Bernal or hexagonal), the *AB′AB′* (i.e., orthorhombic), *ABC ABC* (i.e., rhombohedral), and *AAAA*, the Bernal type is the most commonly found in nature [96, 97]. On the other hand, the *AAAA* stacking has not been observed so far in the natural graphite, but it is very common for graphite intercalation compounds such as LiC_6 and KC_8 [97].

Carbyne is a one-dimensional chain-like molecular structure and is representative of the *sp*-hybridization in the lattice. The quasi-crystalline structure consists of carbon chains with double $(=C=C=)_n$ (i.e., cumulenic) or alternating single/triple $(C^{o}=C)_n$ (i.e., polyynic) covalent bonds. Owing to their relatively high chemical reactivity, solid carbyne typically contains significant concentrations of impurities and amorphous carbon [98, 99].

3.2 Hybrid Structures of Boron and Carbon: B_xC_y Solids

The structural and physical properties of the hybrid B_xC_y can be comprehended as an intermediate between those of the boron and carbon allotropes as the stoichiometry (i.e., the atomic ratio of boron to carbon) varies in the lattice. In the boron-rich structures, the properties are expected to exhibit boron-like features and vice versa. In the following sections, we will review the properties of the hybrid B_xC_y in either the boron-rich and carbon-rich phases.

3.2.1 Boron-Rich B_xC_y Solid

Boron carbide (B_4C) is the well-known hybrid solid in which the carbon content can vary from 8 to 20 at.% [100, 101]. It is one of the hardest material after diamond and cubic-BN [102, 103]. In addition to its hardness, B_4C has a high melting point and high resistance to chemical reagents. Because of these properties, thin films [104, 105] of boron carbide are considered as coating materials for high-temperature applications. On the other hand, by utilizing its unique fivefold symmetry (Fig. 6), which is rare in nature, the icosahedral boron carbide crystals of size ranging from 1 to 10 μm have been synthesized [106]. Instead of the amorphous-like boron carbide thin film [105], these B_4C crystals can be used as a tip of a micro or nanoindenter.

The atomic structure of the icosahedral B_4C solid is rather unique [108, 109] (Fig. 6). It consists of the distorted $B_{11}C$ icosahedra located at the corners of a unit cell of rhombohedral Bravais lattice with the space group R_3m. The icosahedra are

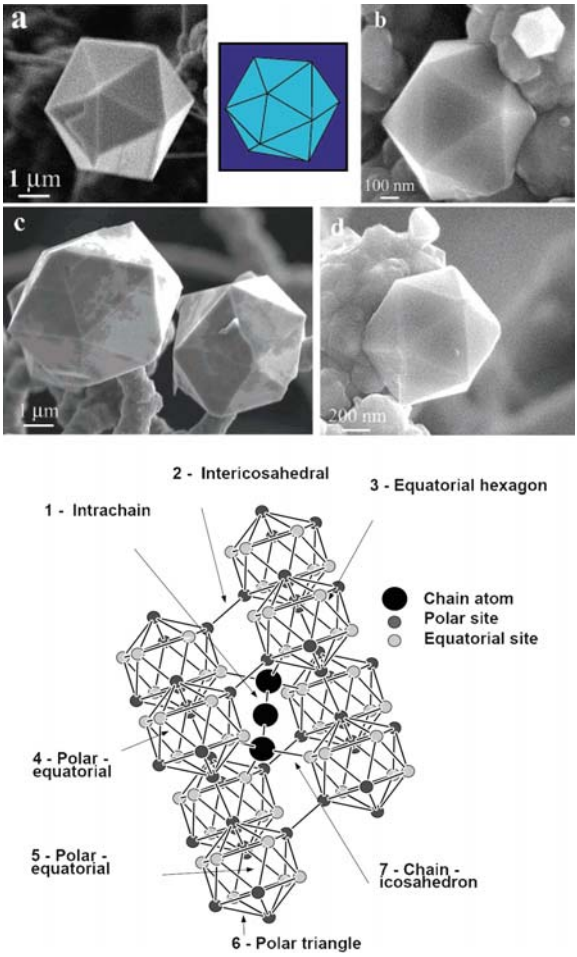

Fig. 6 *Top*: (**a**) SEM image of a typical icosahedron crystal of boron carbide. The diagonal across the crystal is about 5 μm. The inset shows an illustrating model of an isolated icosahedron corresponding to the real crystal. (**b–d**) Icosahedral multiply twinned particles (MTP) crystals observed in the range from 0.5 to 10 μm, with various orientations [106] (reprinted with permission from [106], copyright American Chemical Society). *Bottom*: The atomic structure of B_4C [107] (reprinted with permission from [107], copyright American Physical Society)

connected by the atomic linear chains (e.g., C–B–C) in the lattice [107]. However, the location of the carbon atoms in the $B_{12-n}C_n$ icosahedron and the value of n are still not exactly known [110–112]. This may be due to some degree of randomness, as the *six* equatorial (chain-connected) and the *six* polar (icosahedron-connected) icosahedral sites are indistinguishable in the lattice. It has recently been suggested that the boron carbide solid could be composed of different polytypes, each corresponding to a given possible configuration of chain and icosahedron determined by the

certain degree of randomness [113] that leads to the fluctuation of its stoichiometry. We note here that the effects of polytypes on the mechanical properties (i.e., Hugoniot elastic limit) of the B_4C solid were considered in theoretical study [113] without employing an appropriate stochastic model.

To determine the exact sequence of the chain (i.e., C–B–C, C–B–B, or C–C–C) in the B_4C lattice [114, 115], Raman spectroscopy [116, 117] and FTIR measurements [117] were performed on the amorphous boron carbide (a–B_4C). The results find the preference of the C–B–C chain over the C–C–C chain in the lattice. In particular, the signature of decreased intensity of the infrared stretching mode of C–B–C chains shows that the formation of the a–B_4C lattice may be due to the collapse of $B_{11}C$(CBC) unit of the crystalline lattice through the reorganization into the energetically favorite carbon and boron clusters. However, one needs to perform further studies to completely rule out the possibility of C–C–C and C–B–B chains in the crystalline lattice.

3.2.2 Carbon-Rich B_xC_y Solid

Considering that the stoichiometry determines the structural and electronic properties of a hybrid solid, we expect the structural features of the carbon-rich B_xC_y solids to be dominated by either the sp^2 graphitic or the sp^3 diamond configuration. This is indeed the case for the boron-doped B_xC_{1-x} binary compounds [118–121] having the sp^3 diamond-like tetrahedral networks in the lattice. Diamond, known as the hardest material with the highest atomic density, does not easily incorporate any other dopants in the lattice with exceptions being hydrogen, boron, nitrogen, and silicon. Boron is the only efficient dopant element that can be incorporated with high reproducibility and high enough concentration to be useful for applications of doped diamond in electronic devices [122].

For low-dopant concentrations [118, 119], boron-doped diamond is a p-type semiconductor with carrier concentration of ~10^{17}–10^{19} cm^{-3}. However, the lattice shows metallic-like conductibility [123] for the heavily doped diamond with the dopant concentration of about ≥10^{20} cm^{-3}. Furthermore, superconductivity has been seen in the heavily boron-doped diamond solid [124] and thin films [125, 126]. First-principles calculations [127–132] have tried to elucidate the mechanism responsible for superconductivity in the B_xC_{1-x} compounds. Specifically, the vibrational modes associated with the boron atoms that provide an essential contribution to the *electron–phonon* coupling strength have been identified [132]. The superconducting transition temperature is found to be dependent on the level of the boron doping [127–129]. It has been pointed out that the 3D nature of the network in the boron-doped diamond reduces the density of states at the Fermi level [130] leading to a lower transition temperature as compared to that in MgB_2. Following this observation, study of the B-doped diamond surfaces is now warranted since the 2D nature of the surface states in the lattice may lead to a higher superconducting transition temperature in the boorn-doped diamond.

The signatures of the sp^2 graphitic structural features have been found in the bulk BC_3 [133–135] (Fig. 7), which was synthesized by the chemical reaction of benzene

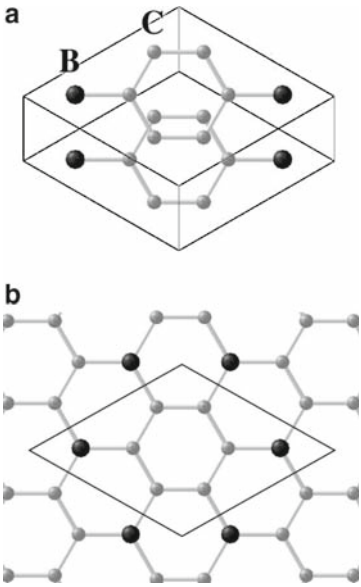

Fig. 7 Top view of the BC_3 structure with the *ABC* stacking. In (**a**) two superimposed unit cells are viewed directly from above and in (**b**) a single layer of atoms is shown (reprinted with permission from [136], copyright American Physical Society)

and boron trichloride at 800°C [137]. Recent theoretical calculations predict the stacking of the BC_3 layers in a hexagonal lattice to be different from that in graphite. The layers in BC_3 prefer a nondirect stacking instead of direct stacking on top of each other [138] in which *ABAB* and *ABC ABC* are predicted to be the energetically stable configurations [138] with real phonon frequencies at Γ *ABAB* being lower in energy by ~1 meV/atom.

In BC_3 (Fig. 7), the calculated in-plane bond length (~5.11–5.12 Å) is independent of the stacking sequence leading to the interatomic sepration of $d_{C–C}$ and $d_{B–C}$ to be ~1.41 and 1.55 Å, respectively [138]. In contrast to the in-plane configuration, the interlayer distance ($c/2$ of *AB AB* or $c/3$ for *ABC ABC*) depends strongly on the stacking type ranging from 3.11 to 3.67 Å. Despite the BC_3 monolayer [134] being a semiconductor with an indirect band gap of ~0.66 eV, the *AB AB* and *ABC ABC* layered bulk are semiconducting with an indirect band gap around 0.5 eV and metallic, respectively. On the other hand, the experimental results [133, 137] find the layered bulk to be metallic. Thus, the layered BC_3 structure, as synthesized experimentally, appears to consist of both stacking configurations. Furthermore, superconductivity in the hole-doped BC_3 was predicted. Because of the strong electron–phonon coupling between the electronic states of the σ band and the phonon modes associated with the bond stretching mode, the superconducting temperature was predicted to increase as a function of the hole doping level in the BC_3 lattice [136].

3.3 Hybrid Structures of Boron and Carbon: B_xC_y Nanostructures

Compared to their precursors in the B_xC_y solid, the properties of the B_xC_y nanostructures are expected to be different due to their "finiteness" in the physical size together with the large surface area to volume ratio. In terms of the system size, the B_xC_y nanostructures are intermediate between molecules and solids consisting of up to a few thousand atoms. In these atomic aggregates nanostructures where the surface plays a paramount role, dependence of the material property on the system size becomes nonscalable [139]. Therefore, exploration of the richness of the unique properties of the hybrid B_xC_y structures in the nanoscale regime will never be a trivial study.

Considering that the research on the novel B_xC_y nanostructures will largely be driven by that on the carbon-based nanostructures, such as fullerene, graphene, and nanotube, we will highlight some of the recent developments in the areas pertaining to physical and chemical properties of carbon nanostructures in the following section.

3.3.1 Carbon Nanostructures

The carbon-based nanostructures, in general, offer new insight into the low-dimensional physics that has never ceased to surprise and continues to provide a fertile ground for novel technological applications. Accordingly, the rapid progress that stems from the novel carbon nanostructures has been evolved into matured subfields of the materials science, such as fullerenes [140–144] and CNTs [91, 92, 141, 145].

Starting from its lowest dimensional case, fullerenes attracted renewed interest owing to the properties of molecular magnets obtained by chemically modifying the structures through the formation of $X@C_{60}$ (i.e., an endohedral fullerene with a X atom encapsulation inside a C_{60} cage). Since the spin of the X atom in $X@C_{60}$ exhibits a low interaction with the environment, a very long spin lifetime (i.e., up to ~0.25 ms) is observed making $X@C_{60}$ to be a promising candidate for qubits in the quantum computation [146, 147]. On the other hand, due to its unique and strong 1D configuration, CNTs are promising building blocks for future nanoscale devices. Single-walled CNTs (SWCNTs) can be metallic or semiconducting depending on the tube diameter and chirality (i.e., the way the graphene sheet rolls up as a seamless hollow cylinder) [91, 92]. Both semiconducting and metallic SWCNTs have been used in advanced electronic devices for single-electron transport [148, 149], spin transport [150], rectification [151, 152], and switching [153].

The role played by graphene, composed of a carbon atomic layer extended in a perfect 2D crystalline lattice, is also becoming remarkably important. Acting as a basic building block for all sp^2 graphitic carbon materials [154], graphene has led to the emergence of a new paradigm of "relativistic" condensed matter physics and "quantum electrodynamics" effects, which can now be tested in the tabletop experiments [154, 155]. In addition to the unusual electronic properties, the thermal conductivity

and mechanical stiffness of graphene may rival the in-plane values for graphite, i.e., ~3,000 W m^{-1} K^{-1} and 1,060 GPa, respectively. The fracture strength should also be comparable to that of CNTs [156–158]. As a next step toward the potential applications, a general approach for the preparation of a graphene in a polymer matrix with intriguing properties has been found via complete exfoliation of graphite and molecular-level dispersion of individual, chemically modified graphene sheets [159].

Graphene has an exceptional advantage that can complement C_{60}, CNTs, and their derivatives. C_{60} is a fascinating molecule, but useful material tends to be extended in at least one dimension. For CNTs, working as long, thin, good molecular transistor is adequate, but microelectronics design is inherently the case of 2D. Yet, issues such as diameter, chirality control, and cost of production pose severe challenges for the commercial applications of CNTs. Graphene appears to be the material that we wished all along for novel technological applications.

3.3.2 B_xC_y Hybrid Nanostructures

The study of the B_xC_y hybrid nanostructures has been driven largely by both scientific curiosity and technological applications. Synthesis of both 0D and 1D B_xC_y nanostructures can be found in the scientific literature. On the other hand, the 2D B_xC_y hybrid nanostructures, such as the semiconducting BC_3 monolayer, remain merely a focus of theoretical studies [134].

Stimulated by the discovery of carbon fullerenes, the so-called heterofullerenes [160–162], where a few C atoms are substituted by hetero atoms, have become of focus of recent research activities. Substitution of dopant atoms such as B, Si, and N into fullerenes is expected to produce significant variation in the electronic structure of fullerene with the possibility of the new type of physical properties, just like the case of doped diamond. Using the method of the laser-vaporization of a graphite/boron nitride composite disk, the first report of the existence of B_xC_{60-x} fullerene-like cage clusters in gas phase was made [160]. Henceforth, the B-*doped* fullerenes have been studied extensively [163–165], either in the forms of films [165], or through in situ electron irradiation of chemical vapor deposition on B_xC_{1-x} ($x \leq 0.2$) [164].

On the other hand, 1D "bulk-like" B_xC_y nanowires have been synthesized due to their attractive properties for high-temperature applications. Besides the formation of amorphous helical boron carbide nanowires [166], the formation of crystalline B_4C nanowires was also reported [167]. Grown by the plasma-enhanced chemical vapor deposition on the (100)-oriented silicon substrates within the range of 1,100–1,200°C, the crystallinity of the B_4C nanowire has been proven by the Raman and near-edge X-ray absorption fine structure spectroscopy. The predominant sp^3 character suggests that the nanowires are extremely hard. We note that the B_4C nanowires (or nanorods) can also be synthesized directly from CNTs at around 1,200°C [168, 169]. The 1D B_xC_y hybrid nanostructures can also be formed via boron doping of CNTs [164, 170–172]. For example, synthesis of multiwalled B_xC_{1-x} ($x \sim 0.1$) nanotubules [164] and the BC_{35} B-doped CNTs [170] has been

reported. A method involving the partial substitution of the carbon atoms on CNTs with B_2O_3 was also proposed [171].

The B-doped CNTs are found to be metallic with no apparent band gap [172]. In the measurements of the resistivity of pristine and B-doped CNTs, it has been shown that the B-doped nanotubes have a reduced room-temperature resistivity with ~7.4×10^7 to 7.7×10^6 Ωm, as compared to that of the pristine nanotubes in the range of 5.3×10^6 to 1.9×10^5 Ωm [173]. Thus, it appears that the metallicity of CNTs can be enhanced by increasing the doping concentration of boron. Consequently, as the ratio of boron is comparable to carbon approaching B/C = 1, the possibility of the existence of the hybrid BC nanotube has recently been supported by a theoretical study [174]. We expect the experimental verification of the BC hybrid tubular configuration in near future, thus expanding the current list of known B_xC_y hybrid nanostructures.

4 Summary

The present research status of the B_xC_y hybrid structures has been reviewed in this chapter. We find that the B_xC_y hybrid structures in either the bulk phase or the nanoscale regime are unique in many aspects. There is also a strong evidence to show that the synthesis of B_xC_y hybrid structures requires an ability to control the bonding between boron and carbon in the lattice. A detailed and systematic understanding of the elemental boron and its derivatives is also warranted.

Owing to its unique features of electron-deficient bonding, both boron solids and nanostructures seem to generally favor a mixture of localized (i.e., two-center) and delocalized (i.e., three-center or multicenter bonds) bonds in the bonding topology. In contrast to carbon, several metastable competing structural motifs can be found in boron nanostructures (e.g., nanotubes and boron sheets), reminiscent of its polymorphism in the solid state. Hence, polymorphism appears to be one of the stumbling blocks associated with synthesis of boron nanostructures. There is an acute need for more systematic and detailed studies on the elemental boron spanning dimensionality from 0D to 3D. With the help of such theoretical and experimental studies, our goal of a complete understanding of the B_xC_y system can be achieved.

References

1. W. Kohn, Rev. Mod. Phys. **71**, S59 (1999).
2. Y.K. Yap, Boron-carbon nitride nanohybrids, In: H.S. Nalwa (Ed.) *Encyclopedia of Nanoscience and Nanotechnology*, **1**, 383–394 (American Scientific, New York, 2004).
3. A.R. Badzian, T. Niemyski, S. Appenheimer, and E. Olkusnik, In: F.A. Claski (Ed.) *Proceedings of the Third International Conference on Chemical Vapor Deposition* (Edited by F.A. Claski), 747 (1972).
4. E.L. Muetterties (Ed.), *The Chemistry of Boron and Its Compounds* (John Wiley, New York, 1967).
5. E.L. Muetterties (Ed.), *Boron Hydride Chemistry* (Academic, New York, 1975).

6. L. Pauling, *Nature of Chemical Bond and the Structure of Molecules and Crystals*, *3rd* Edition (Cornell University Press, Itacha, NY, 1960).
7. A. Quandt and I. Boustani, ChemPhysChem **6**, 2001 (2005).
8. K.C. Buschbeck, *Boron Compounds, Elemental Boron, and Boron Carbides*, *Gmelin Handbook of Inorganic Chemistry*, Vol. 13 (Springer, Berlin, 1981).
9. D.W. Bullett, J. Phys. C Solid State Phys. **15**, 415 (1982).
10. C. Mailhiot, J.B. Grant, and A.K. McMahan, Phys. Rev. B **42**, 9033 (1990).
11. D. Li, Y. Xu, and W.Y. Ching, Phys. Rev. B **45**, 5895 (1992).
12. N. Vast, S. Baroni, G. Zerah, J.M. Besson, A. Polian, J.C. Chervin, and T. Grimsditch, Phys. Rev. Lett. **78**, 693 (1997).
13. M. Fujimori, T. Tanaka, T. Nakayama, E. Nishibori, K. Kimura, M. Takata, and M. Sakata, Phy. Rev. Lett. **82**, 4452 (1999).
14. J. Zhao and J.P. Lu, Phys. Rev. B **66**, 092101 (2002).
15. U. Häussermann, S.I. Simak, R. Ahuja, and B. Johansson, Phys. Rev. Lett **90**, 065701 (2003).
16. A. Masago, K. Shirai, and H. Katayama-Yoshida, Phys. Rev. B **73**, 104102 (2006).
17. R.J. Nelmes, J.S. Loveday, D.R. Allan, J.M. Besson, G. Hamel, P. Grima, and S. Hull, Phys. Rev. B **47**, 7668 (1993).
18. J.C. Thompson and W.J. McDonald, Phys. Rev. **132**, 82 (1963).
19. D.N. Sanz, P. Loubeyre, and M. Mezouar, Phys. Rev. Lett. **89**, 245501 (2002).
20. D.A. Young, *Phase Diagrams of the Elements* (University of California Press, Berkeley, CA, 1991).
21. R. Kawai and J.H. Weare, J. Chem. Phys. **95**, 1151 (1991).
22. R. Kawai and J.H. Weare, Chem. Phys. Lett. **191**, 311 (1992).
23. H.C. Longuet-HigginsM. de. V. Roberts, Proc. R. Soc. Lond. Ser. A **A224**, 336 (1955).
24. H.C. Longuet-Higgins, Q. Rev. Chem. Soc. **11**, 121 (1957).
25. K.C. Lau and R. Pandey, J. Phys. Chem. C, **111**, 2906 (2007).
26. M.I. Eremets, V.V. Struzhkin, H.K. Mao, and R.J. Hemley, Science **293**, 272 (2001).
27. T.H. Geballe, Science **293**, 223 (2001).
28. D.A. Papaconstantopoulos and M.J. Mehl, Phys. Rev. B **65**, 172510 (2002).
29. W.N. Lipscomb, *Boron Hydrides* (Benjamin, New York, 1963).
30. W.N. Lipscomb, J. Less Common Met. **82**, 1 (1981).
31. E.D. Jemmis, M.M. Balakrishnarajan, and P.D. Pancharatna, J. Am. Chem. Soc. **123**, 4313 (2001).
32. E.D. Jemmis, M.M. Balakrishnarajan, and P.D. Pancharatna, Chem. Rev. **102**, 93 (2002).
33. E.D. Jemmis and E.G. Jayasree, Acc. Chem. Res. **36**, 816 (2003).
34. L. Hanley and S.L. Anderson, J. Phys. Chem. **91**, 5161 (1987).
35. L. Hanley, J.L. Whittena, and S.L. Anderson, J. Phys. Chem. **92**, 5803 (1988).
36. S.J. La Placa, P.A. Roland, and J.J. Wynne, Chem. Phys. Lett. **190**, 163 (1992).
37. P.A. Hintz, M.B. Sowa, S.A. Ruatta, and S.L. Anderson, J. Chem. Phys. **94**, 6446 (1991).
38. R. Kawai and J.H. Weare, J. Chem. Phys. **95**, 1151 (1991).
39. R. Kawai and J.H. Weare, Chem. Phys. Lett. **191**, 311 (1992).
40. M.B. Sowa, A.L. Snolanoff, A. Lapicki, and S.L. Anderson, J. Chem. Phys. **106**, 9511 (1997).
41. H.J. Zhai, B. Kiran, J. Li, and L.S. Wang, Nat. Mater. **2**, 827 (2003).
42. B. Kiran, S. Bulusu, H. Zhai, S. Yoo, X.C. Zeng, and L.S. Wang, Proc. Natl Acad. Sci. USA **102**, 961 (2005).
43. C.J. Otten, O.R. Lourie, M. Yu, J.M. Cowley, M.J. Dyer, R.S. Ruoff, and W.E. Buhro, J. Am. Chem. Soc. **124**, 4564 (2002).
44. T.T. Xu, J. Zheng, N. Wu, A.W. Nichollas, J.R. Roth, D.A. Dikin, and R.S. Ruoff, Nano Lett. **4**, 963 (2004).
45. D. Ciuparu, R.F. Klie, Y. Zhu, and L. Pfefferle, J. Phys. Chem. B **108**, 3967 (2004).
46. I. Boustani, Phys. Rev. B **55**, 16426 (1997).
47. I. Boustani and A. Quandt, Europhys. Lett. **39**, 527 (1997).
48. K.C. Lau and R. Pandey, Comput. Lett. (Special Issue: Clusters: From a few atoms to nanoparticles) **1**, 259 (2005).
49. N.G. Szwacki, A. Sadrzadeh, and B.I. Yakobson, Phys. Rev. Lett. **98**, 166804 (2007).
50. A.K. Ray, I.A. Howard, and K.M. Kanal, Phys. Rev. B **45**, 14247 (1992).

51. V. Bonacic-Koutecky, P. Fantucci, and J. Koutecky, Chem. Rev. **91**, 1035 (1991).
52. H. Kato, K. Yamashita, and K. Morokuma, Chem. Phys. Lett. **190**, 361 (1992).
53. I. Boustani, Int. J. Quant. Chem. **52**, 1081 (1994).
54. I. Boustani, Chem. Phys. Lett. **240**, 135 (1995).
55. A. Ricca and C.W. Bauschlicher, Chem. Phys. 208, 233 (1996).
56. F.L. Gu, X. Yang, A.C. Tang, H. Jiao, and P.V.R. Schleyer, J. Comput. Chem. **19**, 203 (1998).
57. J.E. Fowler and J.M. Ugalde, J. Phys. Chem. A 104, 397 (2000).
58. H.J. Zhai, L.S. Wang, A.N. Alexandrova, A.I. Boldyrev, and V.G. Zakrzewski, J. Phys. Chem. A **107**, 9313 (2003).
59. H.J. Zhai, L.S. Wang, A.N. Alexandrova, and A.I. Boldyrev, J. Chem. Phys. **117**, 7917 (2002).
60. A.N. Alexandrova, A.I. Boldyrev, H.J. Zhai, L.S. Wang, E. Steiner, and P.W. Fowler, J. Phys. Chem. A **107**, 1359 (2003).
61. A.N. Alexandrova, A.I. Boldyrev, H.J. Zhai, and L.S. Wang, J. Phys. Chem. A **108**, 3509 (2004).
62. H.J. Zhai, A.N. Alexandrova, K.A. Birch, A.I. Boldyrev, and L.S. Wang, Angew. Chem. Int. Ed. **42**, 6004 (2003).
63. J.E. Fowler and J.M. Ugalde, J. Phys. Chem. A **104**, 397 (2000).
64. J. Aihara, J. Phys. Chem. A **105**, 5486 (2001).
65. M.A.L. Marques and S. Botti, J. Chem. Phys. **123**, 014310 (2005).
66. K.C. Lau, M.D. Deshpande, R. Pati, and R. Pandey, Int. J. Quant. Chem. **103**, 866 (2005).
67. S. Chacko, D.G. Kanhere, and I. Boustani, Phys. Rev. B **68**, 035414 (2003).
68. I. Boustani, A. Rubio, and J.A. Alonso, Chem. Phys. Lett. **311**, 21 (1999).
69. I. Boustani, A. Quandt, and A. Rubio, J. Solid State Chem. **154**, 269 (2000).
70. R.O. Jones and G. Seifert, Phys. Rev. Lett. **79**, 443 (1997).
71. R.O. Jones, J. Chem. Phys. **110**, 5189 (1999).
72. H. Prinzbach, A. Weiler, P. Landenberger, F. Wahl, J. Worth, L.T. Scott, M. Gelmont, D. Olevano, and B. Issendorff, Nature **407**, 60 (2000).
73. N.G. Szwacki, Nanoscale Res. Lett. **3**, 49 (2008).
74. M.H. Evans, J.D. Joannopoulos, and S.T. Pantelides, Phys. Rev. B **72**, 045434 (2005).
75. I. Cabria, M.J. López, and J.A. Alonso, Nanotechnology **17**, 778 (2006).
76. K.C. Lau and R. Pandey, J. Phys. Chem. B, **112**, 10217 (2008).
77. J. Kunstmann and A. Quandt, Phys. Rev. B **74**, 035413 (2006).
78. H. Tang and S. Ismail-Beigi, Phys. Rev. Lett. **99**, 115501 (2007).
79. X. Yang, Y. Ding, and J. Ni, Phys. Rev. B **77**, 041402(R) (2008).
80. K.C. Lau, R. Pati, A.C. Pineda, and R. Pandey, Chem. Phys. Lett. **418**, 549 (2006).
81. K.C. Lau, R. Orlando, and R. Pandey, J. Phys. Condens. Matter **20**, 125202 (2008).
82. K. Kirihara, Z. Wang, K. Kawaguchi, Y. Shimizu, T. Sasaki, N. Koshizaki, K. Soga, and K. Kimura, Appl. Phys. Lett. **86**, 212101 (2005).
83. I. Boustani, A. Quandt, E. Hernández, and A. Rubio, J. Chem. Phys. **110**,3176 (1999).
84. J. Kunstmann and A. Quandt, Chem. Phys. Lett. **402**, 21 (2005).
85. D. Zhang, R. Zhu, and C. Liu, J. Mater. Chem. **16**, 2429 (2006).
86. K.C. Lau, R. Pandey, R. Pati, and S.P. Karna, Appl. Phys. Lett. **88**, 212111 (2006).
87. S. Reich, C. Thomsen, and P. Ordejon, Phys. Rev. B **65**, 153407 (2002).
88. J. Tang, L. Qin, T. Sasaki, M. Yudasaka, A. Matsushita, and S. Iijima, Phys. Rev. Lett. **85**, 1887 (2000).
89. C. Kittel, *Introduction to Solid State Physics*, *7th* Edition (Wiley, New York, 1996).
90. R.B. Heimann, S.E. Evsyukov and Y. Kocack, *Proc. Fifth London Int. Carbon Graphite Conf.* **3**, 104 (1979).
91. R. Saito, G. Dresselhaus, and M.S. Dresselhaus, *Physical Properties of Carbon Nanotubes* (Imperial College Press, London, 2003).
92. M.S. Dresselhaus, G. Dresselhaus, and P. Avouris (Eds.) *Carbon Nanotubes: Synthesis, Structure, Properties, and Applications* (Springer, Berlin, 2001).
93. F.P. Bundy and J.S. Kasper, J. Chem. Phys. **46**, 3437 (1967).
94. T. Yagi, W. Utsumi, M. Yamakata, T. Kikegawa, and O. Shimomura, Phys. Rev. B **46**, 6031 (1992).
95. H. Rydberg, M. Dion, N. Jacobson, E. Schröder, P. Hyldgaard, S.I. Simak, D.C. Langreth, and B.L. Lundqvist, Phys. Rev. Lett. **91**, 126402 (2003).

96. K. Yoshizawa, T. Yumura, T. Yamabe, and S. Bandow, J. Am. Chem. Soc. **122**, 11871 (2000).
97. M.S. Dresselhaus and G. Dresselhaus, Adv. Phys. **51**, 1 (2002).
98. Y.P. Kudryavtsev, S.E. Evsyukov, M.B. Guseva, V.G. Babaev, and V.V. Khvostov, Russ. Chem. Bull. **42**, 399 (1993).
99. B.V. Lebedev, Russ. Chem. Bull. **49**, 965 (2000).
100. C.X. Shi and J. Ke (Eds.) *Structure and Properties of Ceramics, Materials Science and Technology*, Vol. 11 (Science Press, Beijing, 1998).
101. G.V. Tsagareishvili and F.N. Tavatze, Prog. Cryst. Growth Char. **16**, 341 (1988).
102. H.T. Hall and L.A. Compton, Inorg. Chem. **4**, 1213 (1965).
103. S. Han, J. Ihm, S.G. Louie, and M.L. Cohen, Phys. Rev. Lett. **80**, 997 (1998).
104. K.L. Saenger, Angular distribution of ablated material, In: D.B. Chrisey and G.K. Hubler (Eds.) *Pulsed Laser Deposition of Thin Films* (Wiley, New York, 1994).
105. F. Kokai, M. Taniwaki, T. Takahashi, A. Goto, M. Ishihara, K. Yamamoto, and Y. Koga, Diamond Relat. Mater. **10**, 1412 (2001).
106. B. Wei, R. Vajtai, Y.J. Jung, F. Banhart, G. Ramanath, and P.M. Ajayan, J. Phys. Chem. B **106**, 5807 (2002).
107. R. Lazzari, N. Vast, J.M. Besson, S. Baroni, and A.D. Corso, Phys. Rev. Lett. **83**, 3230 (1999).
108. J. Donohue, *The Structure of the Elements* (Wiley, New York, 1974).
109. H.L. Yakel, Acta Crystallogr. B **31**, 1797 (1975).
110. F. Mauri et al., Phys. Rev. Lett. **87**, 085506 (2001).
111. Y. Feng et al., Phys. Rev. B **69**, 125402 (2004).
112. P. Lunca-Popa et al., J. Phys. D **38**, 1248 (2005).
113. G. Fanchini, J.W. McCauley, and M. Chhowalla, Phys. Rev. Lett. **97**, 035502 (2006).
114. T.M. Duncan, J. Am. Chem. Soc. **106**, 2270 (1984).
115. D.M. Bylander et al., Phys. Rev. B **42**, 1394 (1990).
116. X.Q. Yan, W.J. Li, T. Goto, and M.W. Chen, Appl. Phys. Lett. **88**, 131905 (2006).
117. D. Ghosh, G. Subhash, C.H. Lee, and Y.K. Yap, Appl. Phys. Lett. **91**, 061910 (2007).
118. R.M. Chrenko, Phys. Rev. B. **7**, 4560 (1970).
119. R. Kalish, Diamond Relat. Mater. **10**, 1749 (2001).
120. J.E. Butler, M.W. Geis, K.E. Krohn, J. LawlessJr., S. Deneault, T.M. Lyszczarz, D. Flechtner, and R. Wright, Semicond. Sci. Technol. **18**, S67 (2003).
121. J. Robertson, Semicond. Sci. Technol. **18**, S12 (2003).
122. K. Thonke, Semicond. Sci. Technol. **18**, S20 (2003).
123. M. Werner, O. Dorsch, H.U. Baerwind, E. Obermeier, L. Haase, W. Seifert, A. Ringhandt, C. Johnston, S. Romani, H. Bishop, and R.P. Chalker, Appl. Phys. Lett. **64**, 595 (1994).
124. E.A. Ekimov, V.A. Sidorov, E.D. Bauer, N.N. Mel'nik, N.J. Curro, J.D. Thompson, and S.M. Stishov, Nature **428**, 542 (2004).
125. Y. Takano, M. Nagao, I. Sakaguchi, M. Tachiki, T. Hatano, K. Kobayashi, H. Umezawa, and H.H. Kawarada, Appl. Phys. Lett. **85**, 2851 (2004).
126. Z.L. Wang, Q. Luo, L.W. Liu, C.Y. Li, H.X. Yang, H.F. Yang, J.J. Li, X.Y. Lu, Z.S. Jin, L. Lu, and C.Z. Gu, Diamond Relat. Mater. **15**, 659 (2006).
127. L. Boeri, J. Kortus, and O.K. Anderson, Phys. Rev. Lett. **93**, 237002 (2004).
128. K.W. Lee and W.E. Pickett, Phys. Rev. Lett. **93**, 237003 (2004).
129. E. Bustrarret, J. Kacmarcik, C. Marcenat, E. Gheeraert, C. Cytemann, J. Marcus, and T. Klein, Phys. Rev. Lett. **93**, 237005 (2004).
130. X. Blase, Ch. Adessi, and D. Connetable, Phys. Rev. Lett. **93**, 237004 (2004).
131. H.J. Xiang, Z. Li, J. Yang, J.G. Hou, and Q. Zhu, Phys. Rev. B **70**, 212504 (2004).
132. F. Giustino, J.R. Yates, I. Souza, M.L. Cohen, and S.G. Louie, Phys. Rev. Lett. **98**, 047005 (2007).
133. K.M. Krishnan, Appl. Phys. Lett. 58, 1857 (1991).
134. D. Tomanek, R.M. Wentzcovitch, S.G. Louie, and M.L. Cohen, Phys. Rev. B **37**, 3134 (1988).
135. Q. Wang, L. Chen, and J.F. Annett, Phys. Rev. B **54**, R2271 (1996).
136. F.J. Ribeiro and M.L. Cohen, Phys. Rev. B **69**, 212507 (2004).
137. J. Kouvetakis, R.B. Kaner, M.L. Sattler, and N. Bartlett, J. Chem. Soc. Chem. Commun. 1758 (1986).

138. H. Sun, F.J. Ribeiro, J. Li, D. Roundy, M.L. Cohen, and S.G. Louie, Phys. Rev. B **69**, 024110 (2004).
139. U. Landman and W.D. Luedtke, Faraday Discuss. Chem. Soc. **125**, 1 (2004).
140. H.W. Kroto, J.R. Heath, S.C. O'Brien, R.F. Curl, and R.E. Smalley, Nature **318**, 162 (1985).
141. M.S. Dresselhaus, G. Dresselhaus, and P.C. Ecklund, *Science of Fullerenes and Carbon Nanotubes* (Academic, San Diego, 1996).
142. H.W. Kroto, J.E. Fischer, and D.E. Cox (Eds.) *The Fullerenes* (Pergamon, Oxford, 1993).
143. H.W. Kroto and D.R.M. Walton (Eds.), *The Fullerenes, New Horizons for the Chemistry, Physics, and Astrophysics of Carbon* (Cambridge University Press, Cambridge, 1993).
144. L. Forro and L. Mihaly, Rep. Prog. Phys. **64**, 649 (2001).
145. S. Iijima, Nature 354, 56 (1991).
146. J.J.L. Morton, A.M. Tyryshkin, A. Ardavan, K. Porfyrakis, S.A. Lyon, and G.A.D. Briggs, Nat. Phys. **2**, 40 (2006).
147. S.C. Benjamin, A. Ardavan, G.A.D. Briggs, D.A. Britz, D. Gunlycke, J. Jefferson, M.A.G. Jones, D.F. Leigh, B.W. Lovett, A.N. Khlobystov, S.A. Lyon, J.J.L. Morton, K. Porfyrakis, M.R. Sambrook, and A.M. Tyryshkin, J. Phys. Condens. Matter. **18**, S867 (2006).
148. S.J. Tan, M.H. Devoret, H. Dai, A. Thess, R.E. Smalley, L.J. Geerligs, and C. Dekker, Nature **386**, 474 (1997).
149. M. Bockrath, D.H. Cobden, P.L. McEuen, N.G. Nasreen, G. Chopra, A. Zettl, A. Thess, and R.E. Smalley, Science **275**, 1992 (1997).
150. K. Tsukagoshi, B.W. Alphenaar, and H. Ago, Nature **401**, 572 (1999).
151. Z. Yao, H.W.Ch. Postma, L. Balents, and C. Dekker, Nature **402**, 273 (1999).
152. R.D. Antonov and A.T. Johnson, Phys. Rev. Lett. **83**, 3274 (1999).
153. S.J. Tan, A.R.M. Verschueren, and C. Dekker, Nature **393**, 49 (1998).
154. A.K. Geim and K.S. Novoselov, Nat. Mater. **6**, 183 (2007).
155. M.I. Katsnelson and K.S. Novoselov, Solid State Commun. **143**, 3 (2007).
156. M.S. Dresselhaus and G. Dresselhaus, Adv. Phys. **51**, 1 (2002).
157. M. Hirata, T. Gotou, S. Horiuchi, M. Fujiwara, and M. Ohba, Carbon **42**, 2929 (2004).
158. M.F. Yu, O. Lourie, K. Moloni, T.F. Kelly, and R.S. Ruoff, Science **287**, 637 (2000).
159. S. Stankovich, D.A. Dikin, G.H.B. Dommett, K.M. Kohlhaas, E.J. Zimney, E.A. Stach, R.D. Piner, S.T. Nguyen, and R.S. Ruoff, Nature **442**, 282 (2006).
160. T. Guo, C. Jin, and R.E. Smalley, J. Phys. Chem. **95**, 4948 (1991).
161. R. Yu, M. Zhan, D. Cheng, S. Yang, Z. Liu, and L. Zheng, J. Phys. Chem. **99**, 1818 (1995).
162. J.C. Hummelen, B. Knight, J. Pavlovich, R. Gonzalez, and F. Wudl, Science, **269**, 1554 (1995).
163. T. Kimura, T. Sugai, and H. Shinohara, Chem. Phys. Lett. **256**, 269 (1996).
164. D. Golberg, Y. Bando, K. Kurashima, and T. Sasaki, 72, 2108 (1998).
165. Y.J. Zou, X.W. Zhang, Y.L. Li, B. Wang, H. Yan, J.Z. Cui, L.M. Liu, and D.A. Da, J. Mater. Sci. **37**, 1043 (2002).
166. D.N. Mcllroy, D. Zhang, Y. Kranov, H. Han, A. Alkhateeb, and M.G. Norton, Mater. Res. Soc. Symp. Proc. 739, H5.2 (2003).
167. D.N. Mcllroy, D. Zhang, R.M. Cohen, J. Wharton, Y. Geng, M.G. Norton, G. De Stasio, B. Gilbert, L. Perfetti, J.H. Streiff, B. Broocks, and J.L. McHale, Phys. Rev. B **60**, 4874 (1999).
168. H.J. Dai, E.W. Wong, Y.Z. Lu, S.S. Fan, and C.M. Lieber, Nature **375**, 769 (1995).
169. J. Wei, B. Jiang, Y. Li, C. Xu, D. Wu, and B. Wei, J. Mater. Chem. **12**, 3121 (2002).
170. B.C. Satishkumar, A. Govindraraj, K.R. Harikumar, J.P. Zhang, A.K. Cheetham, and C.N.R. Rao, Chem. Phys. Lett. **300**, 473 (1999).
171. W.Q. Han, Y. Bando, K. Kurashima, and T. Sato, Chem. Phys. Lett. **299**, 368 (1999).
172. D.L. Carroll, Ph. Redlich, X. Blase, J.C. Charlier, S. Curran, P.M. Ajayan, S. Roth, and M. Rühle, Phys. Rev. Lett. **81**, 2332 (1998).
173. B.Q. Wei, R. Spolenak, P. Redlich, M. Ruhle, and E. Arzt, Appl. Phys. Lett. **74**, 3149 (1999).
174. O. Ponomarenko, M.W. Radny, and P.V. Smith, Phys. Rev. B **74**, 125421 (2006).